HAL
open science

Thermophysical properties of n-hexadecane: Combined Molecular Dynamics and experimental investigations

Liudmyla Klochko, Justine Noel, Nicolò R Sgreva, Sebastien Leclerc, Christel Metivier, David Lacroix, Mykola Isaiev

To cite this version:

Liudmyla Klochko, Justine Noel, Nicolò R Sgreva, Sebastien Leclerc, Christel Metivier, et al.. Thermophysical properties of n-hexadecane: Combined Molecular Dynamics and experimental investigations. International Communications in Heat and Mass Transfer, 2022, 137, pp.106234. 10.1016/j.icheatmasstransfer.2022.106234 . hal-03736194

HAL Id: hal-03736194

https://hal.univ-lorraine.fr/hal-03736194v1

Submitted on 22 Jul 2022

HAL is a multi-disciplinary open access archive for the deposit and dissemination of scientific research documents, whether they are published or not. The documents may come from teaching and research institutions in France or abroad, or from public or private research centers.

L'archive ouverte pluridisciplinaire **HAL**, est destinée au dépôt et à la diffusion de documents scientifiques de niveau recherche, publiés ou non, émanant des établissements d'enseignement et de recherche français ou étrangers, des laboratoires publics ou privés.

arXiv:submit/4209670 [physics.app-ph] 14 Mar 2022

Thermophysical properties of n-hexadecane: Combined Molecular Dynamics and experimental investigations

L. Klochko, J. Noel, N. R. Sgreva, S. Leclerc, C. Métivier, D. Lacroix, and M. Isaiev

March 14, 2022

Abstract

Investigating properties of phase change materials (PCMs) is an important issue due to their extensive use in heat storage systems and thermal regulation devices. Improvement of the efficiency of such systems should be based on a better knowledge of the microscopic mechanisms governing the thermal and rheological characteristics of PCMs. This may be accomplished by the use of molecular simulations of the aforementioned quantities and their linkage with macroscale investigations. In this work we studied thermophysical properties of n-hexadecane for different temperatures regimes using molecular dynamics (MD) and carry out several experimental measurements. Particularly, we focused on the evaluation of various reological and thermal properties such as thermal conductivity, κ, viscosity, η, diffusion coefficient, D, and heat capacities C_p and C_v. Special attention was paid for the comparison of the results of simulations with experimental ones.

Keywords: Thermal conductivity, viscosity, molecular dynamics, phase change materials (PCMs)

1 Introduction

Rising of the energy demand as well as challenges related to climate change urge the development of efficient energy storage technologies in accordance with the growth of renewable energies production. In this context phase change materials (PCMs) are essential to store/release heat resulting from several industrial and domestic processes. For example, fabrics for clothing that contain PCMs (such as paraffins) provide an excellent thermal regulation, and reduce the amount of sweat produced by the body. They were used at the 2004 Athens Olympics as a "precool" vest invented by the Australian Institute of Sport [1, 2]. PCMs based systems are also inescapable to increase the efficiency of the storage of thermal energy produced from renewable sources such as solar [3] and geothermal energy [4]. Moreover, PCMs-based storage cells allow to collect industrial wasted energy for further re-usage, e.g. for maintaining appropriate working conditions [5]. The wide range of applications of PCMs-based thermal storage systems can be related to the significant latent heat that can be accumulated and released during the solid/liquid phase transition. Despite a large application potential, the employment of PCMs remains often limited due to the complexity of their efficient application.

The first issue is connected with a relatively small thermal conductivity (κ=0.1-0.5 W/m.K) of the most known PCMs. The latter limits theirs charging/discharging rates during solidification/melting processes. This issue can be overcome with the use of solid nanoparticles [6, 7] or porous medium/solid foam [8] to tailor thermal transport properties of the "composite" material. In this framework, research is currently directed on the macroscale optimization of device's configurations to achieve higher performances [9]. At nano/microscale, improvements are possible through the tuning of PCMs/host matrix interactions in elaborated composite materials.

Another aspect that remains problematic in thermal energy storage systems is the triggering of crystallization in supercooled PCMs. Due to this feature, it is often complicated to recover the stored latent heat at the expected conditions, which causes some issues in temperature-controlled applications [10]. Triggering the nucleation process is a possible way to address this issue [11]. Specifically, it can be performed by providing new nucleation sites adding new solid/liquid interfaces. Moreover, nucleation can be furthermore enhanced when the composite material has appropriate surfaces, for example surfaces with adapted wettability which minimizes the nucleation energy at a given temperature [11].

The above-mentioned strategies for enhancing the efficiency of PCMs-based systems require an understanding of the phenomena that occur at the interface between a PCM and a nanostructured solid, because local changes in properties can be huge in systems with a large interfacial area [12]. Thus, the arrangement of molecules/atoms near to the interface is critical in this respect. For instance, heat and mass transfer are known to be significantly modified at the interfaces between different materials (i.e. solid and liquid ones). Noticeable changes are also reported for properties such as thermal conductivity or enthalpy of melting close to a nanoparticle [13] or at fluid-solid interfaces in porous network [14].

Usually one do not know how the distribution of molecules drives the phase change process. Further research into these pathways is thus essential. On the other hand, a thorough description of the interfacial characteristics demands a correct representation of the bulk PCMs' key features. Atomistic approaches are one possible strategy to determine both structural quantities at the interface and bulk properties in such a situation. Specifically, molecular dynamics (MD) techniques are effective tools for investigating the behavior of various systems based on interactions between individual atoms. As a result, it allow us the investigation of the thermophysical [15, 16, 17], rheological [18, 19, 15], and structural [13, 20] characteristics of PCMs and PCM-based nanocomposites. Howewer, MD simulations require the specification of the suitable interaction potential and its subsequent parametrization. It is clear that the latter should be validated by the correlation with the experimental findings to allow further application for the reliable description of the interfacial properties.

From the experimental viewpoint, many reviews on the properties of bulk PCMs are available in the literature (e.g. [21, 22]). Nevertheless, the provided information is usually very specific, it often focuses on macroscopic thermal properties (melting temperature, latent heat) with partial description in terms of methods and protocols. A full thermo-physical characterization is clearly complex because it involves many skills from different fields such as physics of matter, thermodynamics, mechanics, and chemistry, investigating at small scales [23]. An additional complexity lies in the experimental measurements of PCMs properties under controlled conditions and protocols [21]. As mentioned above, supercooling effects are strongly sensitive to experimental conditions. In some recent works [24, 25], we provide the background for a complete and clearly detailed characterization procedure adapted to PCMs. This experimental background enables to measure thermo-physical properties of PCMs with controlled methodologies and protocols. In this way, beyond the sole validation of one method, numerical and experimental approaches can be complementary and can enrich each other. Nevertheless, the first step to achieve consists in ensuring that the results from the two parts (numerical and experimental) are in agreement.

In this work, we propose to study the n-hexadecane by means of both numerical and experimental approaches. Among the numerous types of PCMs, n-alkanes are considered because of their chemical and thermal stability. n-alkanes are widely used in thermal control and energy storage applications. For example, n-alkanes are of interest in the design of based-on hydrocarbons superconductors [26], and oleophobic surfaces [27]. Moreover, the phase transition temperature of n-alkanes corresponds to the human suitable diapason [28]. Here, we focus on the alkane which combines 16 carbon atoms, also called the hexadecane, whose chemical formula is $C_{16}H_{34}$.

MD techniques have been used to investigate the hexadecane in several works. It has already been shown that the temperature behavior of viscosity, density, and interfacial tension estimated with MD [29] for hexadecane correlates well with recent data [18, 24]. Nonetheless, improving the efficiency of PCMs-based heat capacitors necessitates knowledge of the systems' thermal physical features. There are a limited number of investigations devoted to this subject in this setting. For example, it was recently demonstrated that charged nanoparticles can improve the thermal conductivity of hexadecane, according to Zhao et al [17]. However, such investigations are partial and need additional numerical foundation.

Therefore, the current article is devoted to the MD study of transport and rheological properties as well as structural ones of bulk PCMs. The hexadecane was chosen as ta reference. The obtained results are correlated with experimental ones to demonstrate the applicability of the simulations for the modeling of the bulk properties of the studied system. Due to complexity of the MD simulations of crystallization process close to the phase transition point [30] without crystallization seeds, the theoretical work proposed in this current research is done only in liquid phase and amorphous state. In this study, we explore several features of the researched material throughout a temperature range, including the liquid phase, amorphous state, and liquid/amorphous transition.

The paper is organized as follows: in section 2, the experimental setups and results are presented. In section 3, MD simulation models and tools are detailed. Then, the last sections deal with calculation of thermophysical properties and their comparison to experimentally evaluated counterparts. More specifically, we investigate thermal transport properties (κ and C_p) as well as fluid characteristics of PCMs in liquid phase. Concluding remarks and current perspectives to this work ends the paper.

2 Materials and experimental methods

Several batches of 99% pure hexadecane provided by Merck (CAS number 544-76-3) were studied. The data sheet of the provider indicates a melting temperature of $T_m = 291.15$ K, which is in a good agreement with values given in the literature [31, 32]. However, due to the appearance of undercooling effects, establishing the temperature where the crystallization occurs (T_c) is not easy, leading the possibility to work in $T_c < T_m$ temperature regimes [32, 24].

In order to compare observations obtained with computational methods, the experimental characterization of n-hexadecane presented in this study was done in liquid phase, i.e. at $T > T_m$. Employed techniques and methods used for the characterization were similar to those detailed in [24, 25]. This section aims to recall these techniques as well as the main concepts the used throughout measurements.

2.1 Density

Measurements of density, ρ, were carried out at ambient atmospheric pressure with a DMA 5000M Anton-Paar densimeter on a sample of a liquid hexadecane of volume ~1 mL. The obtained data were collected every 1 K from $T = 313$ K to $T = 292$ K with five minutes of thermal stabilization of the sample volume during each step of lowering temperature. Due to the small volume of material employed in the analysis, such stabilizing time was sufficient in the liquid phase. For the considered experimental temperature range, the density measurements have an accuracy of 5×10^{-6} g cm^{-3}. In addition, the coefficient of thermal expansion α_T at a constant pressure p can be directly deduced from the temperature dependence of the density as follows:

$$\alpha_T = -\frac{1}{\rho\,(T)}\left(\frac{\partial\rho}{\partial T}\right)_p \tag{1}$$

2.2 Thermal conductivity

The thermal conductivity, κ, of n-hexadecane in liquid phase was studied by using the hot tube steady state method [33]. The equipment is made of two coaxial cylinders of different diameter with a gap between them that is totally filled with ~ 18 mL of liquid n-hexadecane. Two thermocouples, which are located at the mid-height of the cylinders, record temperatures T_1 and T_2 at the fluid layer's boundaries, i.e. at the interfaces between the fluid and the inner and outer cylinders, respectively. The inner cylinder is heated by Joule effect while the outer is in contact with a water recirculation maintained at controlled temperature. Once the steady state is reached, the thermal conductivity, κ, was calculated by measuring heat flux and temperature as:

$$\kappa(\bar{T}) = \frac{\rho_e I^2 \ln(r_2/r_1)}{2\pi^2(r_1^2 - (r_1 - d)^2)(T_1 - T_2)}, \tag{2}$$

where temperature $\bar{T} = (T_1 + T_2)/2$ is the mean temperature through the PCM layer, ρ_e is the specific electrical resistivity of the inner cylinder (stainless steel), I is the electrical intensity, r_1 and r_2 are the radii bounding the fluid layer (with $r_1 < r_2$), d is the thickness of the inner cylinder, and $(T_1 - T_2)$ is the temperature variation through the fluid layer. Measurements were done by keeping both temperatures T_1 and T_2 higher than T_m.

2.3 Heat capacity

The heat capacity, C_p, was estimated by differential scanning calorimetry (DSC) method. This technique allows the measurement of heat transfer in a small volume of a liquid n-hexadecane subjected to temperature variations. We used a SETERAM μ-DSC3 evo calorimeter for the temperature range of $T \in [292 - 311]$ K. The temperature was varied by 2 K step increments with a heating/cooling rate of 0.2 K/min between each step. The total heat transmitted to the PCM sample across the temperature variation between two temperature steps is correlated with the heat capacity. The total heat in our studies is calculated by integrating the heat power transferred over time: from the start of a temperature step until there is no longer heat exchange between the PCM sample and the DSC. As a result, each temperature step was kept constant for a long enough period of time (about 2 hours) to ensure that the heat flow was fully dissipated.

2.4 Viscosity

The rheological behaviour of liquid n-hexadecane was investigated with an AR-G2 rheometer (TA Instruments), by using both a plate-plate and a cone-plate geometry. We used a 60 mm diameter plate with a fixed 1000 μm gap between the two plates in the plate-plate geometry. In the cone-plate geometry the cone angle was 2°, the plate diameter was 60 mm, and the gap was fixed at 70 μm. Such a large diameter was chosen for the cone and plate because of the low viscosity of n-hexadecane in a liquid phase. Both geometries produced similar results. Rheometry was done under isothermal conditions via a Peltier plate within a range of 289 K to 313 K. In the liquid phase, we observed Newtonian behavior for hexadecane. Creep tests were thus performed at each temperature by applying a shear stress of 0.1 Pa. Tests lasted around two minutes, assuring a steady state response and a viscosity plateau. The resulting viscosity corresponds to the mean of measurements taken over this plateau.

2.5 Diffusion coefficient

Nuclear magnetic resonance (NMR) was used to quantify the diffusion coefficient (which indicates the mass diffusivity of a liquid hexadecane) at various temperatures ranging from 293 K to 310 K. A split air flow, one from below and one from the side of the sample, has been used to impose the temperature on the sample (600 μL volume). Isothermal conditions were ensured by waiting 30 minutes for the temperature to equilibrate before the acquisition.

Spectra were acquired by a Bruker Avance III HD 300 MHz spectrometer equipped with a Bruker BBO probe. We used a stimulated echo technique with bipolar gradients [34], a diffusion gradient duration of δ=2 ms and a diffusion time interval Δ=200 ms. We acquired several spectra at constant temperature with a power gradient g_p ranging from 9.63 to 471.87 mT m^{-1}.

The collected spectra for different gradients are presented in Fig. 1a. Fig. 1b illustrates the dependency of the spectra area vs. the gradient at various temperatures. We initially ran four scans for each gradient to achieve signal equilibrium, and then we acquired the final spectra by averaging eight additional scans.

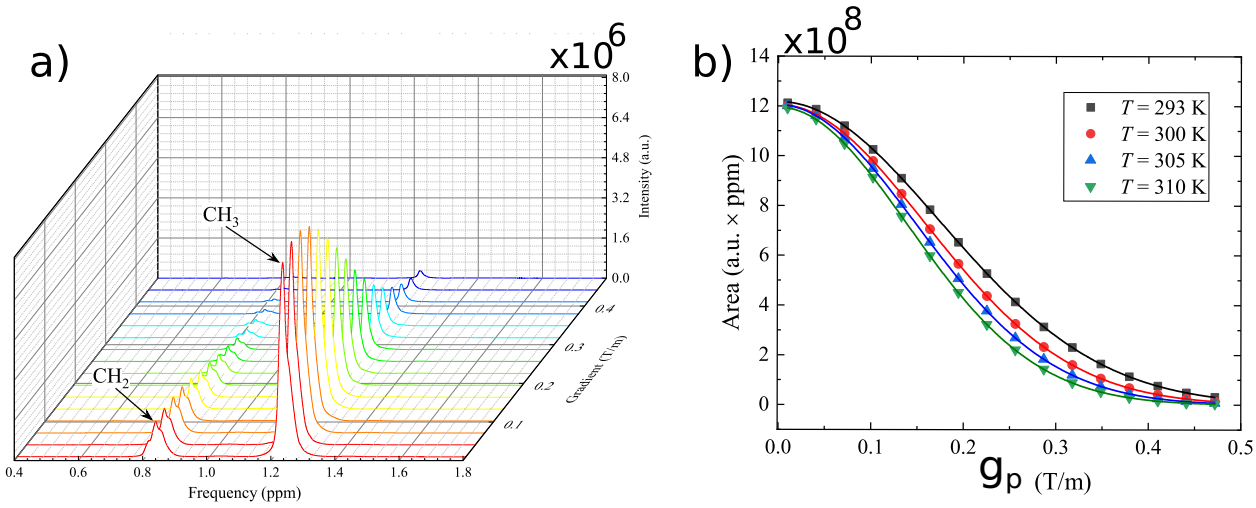

Figure 1: a) Spectra of n-hexadecane at T =293 K for different power gradients, and b) spectra area, A, as a function of power gradient values at different temperatures. Crosses represent the experimental points and solid lines are their fit by following an equation (3).

At a fixed temperature, with the gradient rise, the decrease of intensity of the spectra (see Fig. 1b) can be fitted by the Stejskal-Tanner equation [35] to obtain the diffusion coefficient D:

$$A = A_0 \times \exp(-\gamma^2 g_p^2 \delta^2 D \Delta), \tag{3}$$

where A is the spectrum area, A_0 is the area of a spectrum with a null gradient intensity, and γ is the gyromagnetic ratio of the proton (γ=42.576 MHz T^{-1}).

3 Molecular Dynamics simulations

3.1 Atomistic model for organic compounds

To investigate heat transfer in organic systems one can chose "all-atom" molecular dynamics (MD) algorithm (i.e., each atom of the studied molecule is considered as an individual element in opposite to the coarse-grain method). The latter is used to determine the thermodynamic and rheologic properties of hexadecane. In the following sections we discuss the simulation protocol and the theoretical background that were used to obtain and treat simulation data.

3.2 Simulation protocol

In order to construct a realistic system representative of hexadecane PCMs with randomly distributed molecules we average all our calculations over m=7 distinct initial systems. Each of them is built with N = 500 molecules of hexadecane by using Packmol [36] software. Molecules are randomly set inside a cubic box with periodic boundary conditions. A system, in the initial configuration, was visualized with VMD [37, 38] and is represented in Fig. 2.

Here we partly follow the protocol proposed by Morrow et al. [18]. We chose the initial volume to match the experimental densities at different temperatures. The latter are shown in Fig. 4 (see experimental red dots) for an extended range of temperatures: $T \in [310, 276]$ K with steps of 2 K. In order to speed up the packing we increased the box size of simulation cell by 5 Å in each dimension [18].

Molecular dynamics simulations are performed with LAMMPS [39] software with time-step δt=2 fs. As the choice of the force field is a crucial issue, within this work all-atom optimized L-OPLS [40] force field (see Tables. 1– 4 for more detail) was used due to its realistic approximations compared to experiments [18, 41, 42, 43, 44] (see also secs. 2 and 5). In this work the truncation of non-bonded interaction at $r_{\rm cut}$=15 Å was used. Carbon-hydrogen

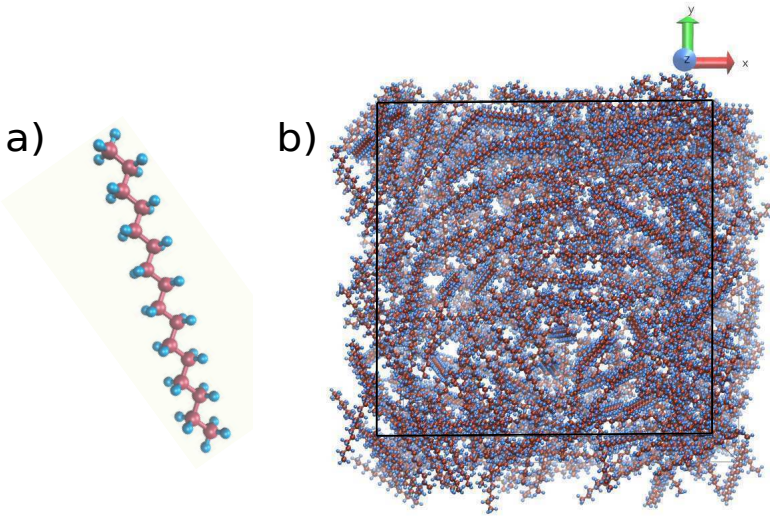

Figure 2: Snapshots of: a) one molecule of n-hexadecane, and b) the initial system of $N = 500$ molecules of n-hexadecane.

bond distances were constrained by applying the SHAKE [45] algorithm. This algorithm apply bond and angle restrictions to given bonds and angles in the simulations, i.e. each timestep specified angles and bonds are reset to their equilibrium values.

Atom	**Partial charge** (e)	σ (Å)	ε (kcal/mol)
C (hexadecane CH_3)	-0.222	3.50	0.06600
C (hexadecane CH_2)	-0.148	3.50	0.06600
H (hexadecane CH_3)	0.074	2.50	0.03000
H (hexadecane CH_2)	0.074	2.50	0.02629

Table 1: Non-bonded parameters for L-OPLS force field [44]

Bond	r_{eq} (Å)	K_b (kcal/mol)
CT-CT	1.529	268
CT-H	1.090	340

Table 2: Bonded parameters for L-OPLS force field [44]

Angle	θ_{eq} (degrees)	K_θ (kcal/mol)
CT-CT-CT	112.7	58.35
CT-CT-H	110.7	37.50
H-CT-H	107.8	33.00

Table 3: Angle parameters for L-OPLS force field [44]

Dihedral	V_1	V_2	V_3
CT-CT-CT-CT	0.6447	-0.2143	0.1782

Table 4: Dihedral Fourier parameters (kcal/mol) for L-OPLS force field [44]

3.3 Liquid/amorphous state, a molecular investigation

The first part of this work is devoted to the characterization of molecular organization of the studied n-hexadecane samples considered in MD simulations used to evaluate thermophysical properties. As mentioned above, crystalline structure of n-hexadecane [17] are scarcely achievable with the simulation parameters used here. Instead, we suggest that amorphous state, characterized by amorphous molecules organization is more probably reached when the calculations are performed below the liquid-solid transition temperature. The purpose of this section is to clarify this point through the use of radial distribution function.

As the solidification process is not changing the initial structure of sample (liquid or solution) it was chosen to calculate radial distribution function (rdf), $g(r)$, of n-haxedecane at low-T and high-T regimes. The main aim of performing such calculations is to observe the possible reorganization of molecule constitutive atoms while the system cross the phase transition temperature, in other words if rdf changes between hot and cold temperature this will be a proof of solidification toward a more organized "quasi-crystalline" state, otherwise this will confirm that the system remains in an amorphous state. Radial distribution function, $g(r)$, can be calculated as:

$$g(r) = \frac{1}{\rho} \left\langle \sum_{i \neq 0} \delta(\boldsymbol{r} - \boldsymbol{r}_i) \right\rangle \tag{4}$$

where $\delta(\boldsymbol{r})$ is the delta function at position $\boldsymbol{r}$.

We calculated the radial distribution function between different types of atoms: i) carbon-carbon atoms in CH_3 and CH_2 groups; ii) hydrogen-hydrogen atoms in in CH_3 and CH_2 groups. Those results for T=310 K and T=272 K are plotted in Fig. 3. As it can be clearly see, rdf peaks remain at the same location, there is only a slight change in their amplitude when T varies. This undoubtedly confirms that no phase transition with a noticeable change of molecules organization occurs. In the achieved simulation our systems for the whole temperature range remain in amorphous state.

3.4 Thermal expansion of the n-hexadecane via MD

Simulations start with energy minimization of the system by updating atom coordinates continuously with the use of "minimize" command in LAMMPS (for more detail see `https://docs.lammps.org/minimize.html`). Then, in a second stage, the simulations are switched in NVT ensemble (where N is the total number of molecules, V and T are the volume and the temperature of the system) for a typical duration of t=245 ps applying Nosé-Hoover thermostat to control temperature [46] and to adjust the chosen volume to the system. Then, in the third stage, in order to reach the desired pressure, p=0.1 MPa, we perform NPT equilibration run for t=4 ns. During the the remaining simulation time t=2 ns, information about densities, ρ, is registered every t = 20 fs.

In Fig. 4 the averaged values of hexadecane density, ρ, obtained by the above detailed simulation procedure are plotted with experimental data obtained by following protocol from subsec. 2.1. As can be seen, the estimated densities are in great agreement with the actual data, which decreases linearly with increasing temperature; our findings are similar with earlier investigations [47]. In the considered temperature range, the calculated error is lower than 5%.

Knowing the temperature dependence of n-hexadecane's density, one can straightforwardly obtain the thermal expansion coefficient α_T (see eq. 1). Using the values of ρ given in Fig. 4 one can obtain $\alpha_T(T)$. The calculated dependence is shown in Fig. 4 for both simulation and experimental data [24, 25]. For similar study [47] was experimentally founded the typical values for density of n-hexadecane in liquid phase (T = 298.15 K) ρ = 770.6 kg m^{-3} that is close to that we obtained within our research. These first results on structural properties (ρ and α_T) of the modelled hexadecane make us confident about the relevance of the chosen atomic model. In the following section, thermal properties will be thus investigated.

4 Calculation of thermophysical properties

For the calculation of thermal conductivity and viscosity of the system, we change slightly the above presented equilibration procedures. Specifically, additional equilibration run in canonical ensemble (NVT) for t =4 ns was performed due to obtain as much equilibrated system as possible. Then, we ensure a long relaxation stage, the system remains in NVT ensemble for t=4 ns instead of 2 ns. Relevant information is saved each t=320 ps for viscosity, μ, each t=80 ps for thermal conductivity κ, and each t=2 ps for total energy of the system, E, entalphy, H, positions, and mean-square displacement.

Achieving such calculations that take into account all the interactions is costly in terms of simulation time and memory resources. We thus perform the above procedure with m=5 independent configurations for each temperature point to achieve the optimum and desired results.

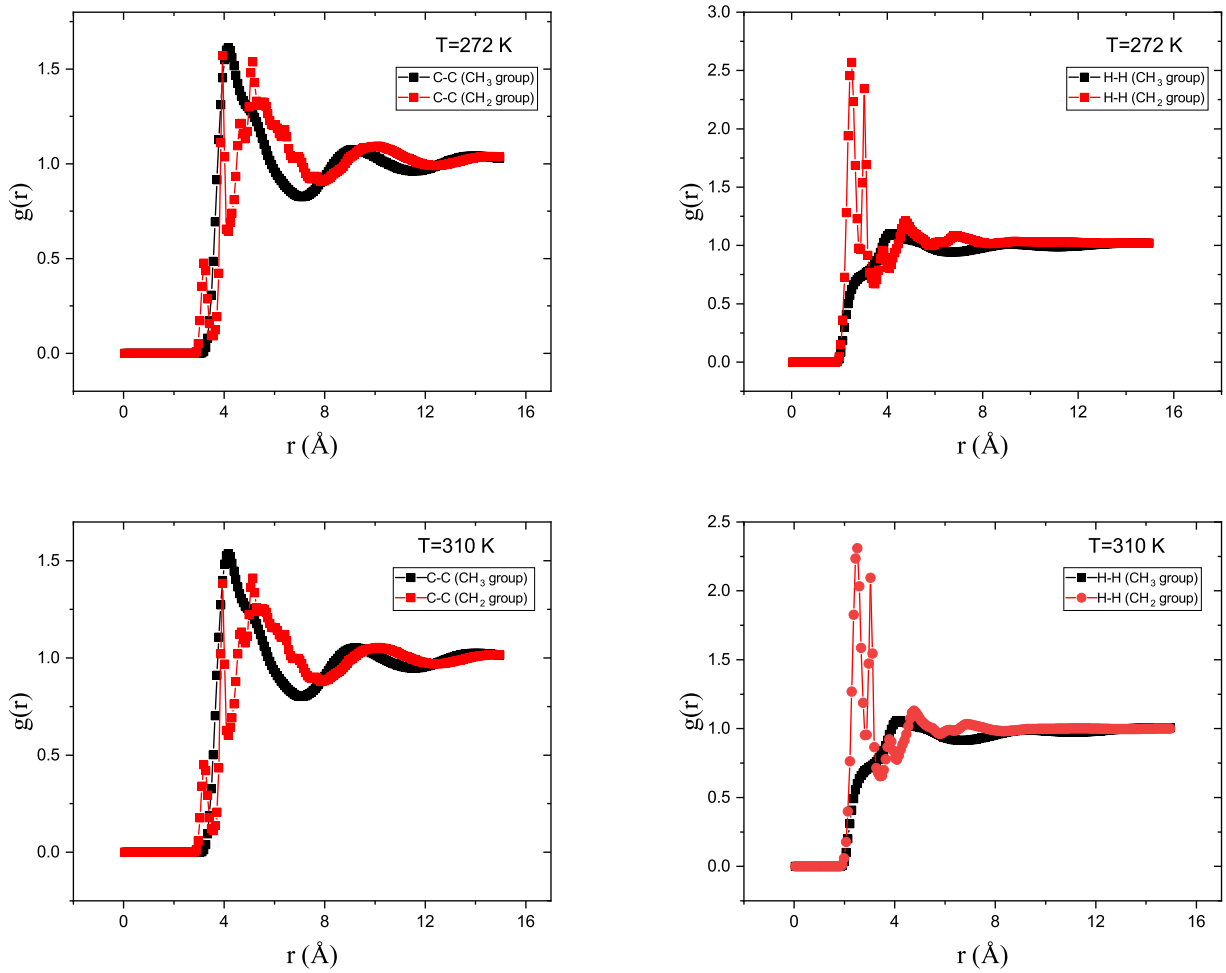

Figure 3: Radial distribution function at $T = 272$ K (top figures) and $T = 310$ K (bottom figures).

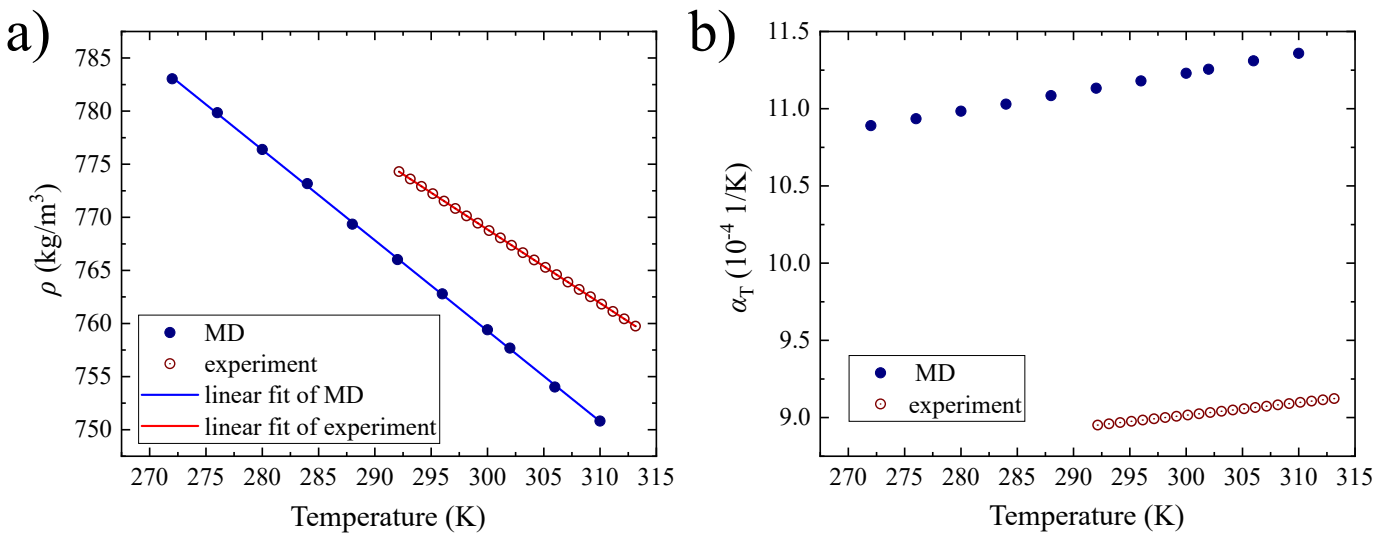

Figure 4: Temperature dependence of hexadecane: a) density, ρ, and b) thermal expansion coefficient, α_T, obtained with MD simulations (blue dots) and experimentally (maroon dots) [24, 25]. Error bars are not indicated due to its insignificance.

4.1 Viscosity and dynamical properties

We used the Green-Kubo method with ensemble average of the auto-correlation of the stress/pressure tensor to calculate viscosity as:

$$\mu = \frac{V}{k_B T} \int_0^\infty \langle \tau_{\alpha\beta}(t)\tau_{\alpha\beta}(0)\rangle \, dt \tag{5}$$

where V is volume of the system, k_B is Boltzman's constant, and $\tau_{\alpha\beta}$ are the non-diagonal elements of the stress tensor ($\alpha\beta$=xy, yz or xz).

Knowing that Eq. 5 can only be used for "well equilibrated" systems (i.e., for simulation time much higher than the relaxation time of the system) with the use of LAMMPS ones has to be sure that steady state is reached. An example of the averaging interval for $\mu(t)$ is shown in Fig. 5 a. In this work, careful evaluation of the "plateau"-like interval was achieved to ensure accurate evaluation of the dynamic viscosity $\mu(t)$ at each desired temperatures. Furthermore, dynamic viscosity of n-hexadecane was measured using plate-plate rheometer controled with Peltier cooling as it was shown in sec 2.4. The comparison between numerical and experimental data is given in Fig. 5. For the latter, agreement is very good on the whole temperature range. Moreover, in literature [47] (at $T = 298.15$ K) calculated viscosity is $\mu = 3.039$ mPa·s. This demonstrate the reliability of the proposed techniques.

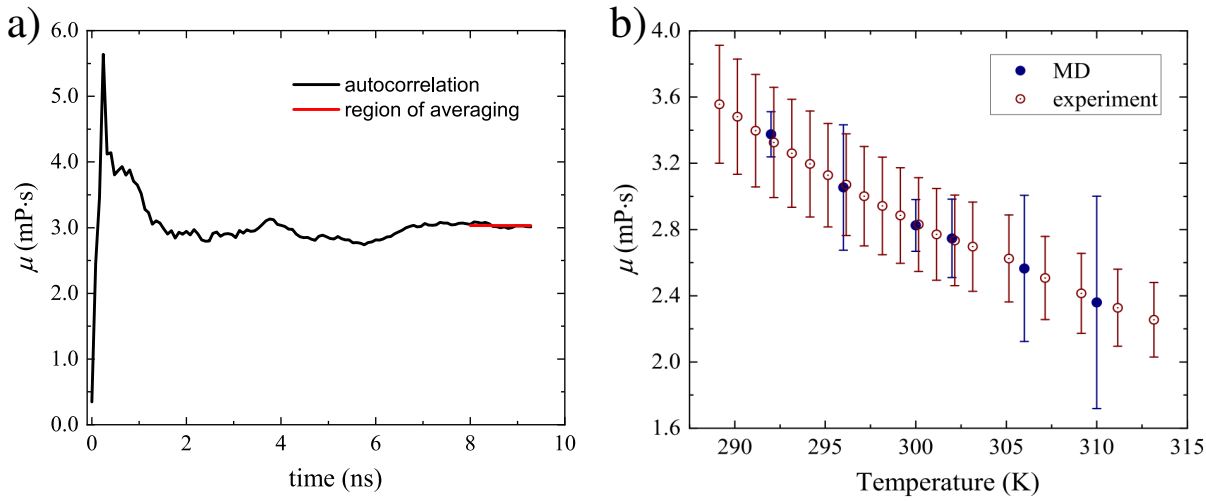

Figure 5: a) Autocorrelation viscosity function obtained for $T = 296$ K. The red line corresponds to the time interval that was used to calculate the mean value shown in Fig. 5 b) and b) dynamic viscosity as a function of temperature.

4.2 Thermal conductivity

Thermal conductivity can be also callated with EMD according to Green-Kubo formalism through the integration of heat flux autocorrelation, as follow:

$$\kappa = \frac{V}{k_B T^2} \int_0^\infty \langle \boldsymbol{J}(t)\, \boldsymbol{J}(0)\rangle \, dt \tag{6}$$

where V is the volume of the system at temperature T, k_B is the Boltzmann constant, and $\boldsymbol{J}(t)$ is the heat flux vector at time t, that can be obtained from:

$$\boldsymbol{J} = \frac{1}{V}\Big[\sum_i \boldsymbol{e}_i \boldsymbol{v}_i - \frac{1}{2}\sum_{i<j} \boldsymbol{F}_{ij}\cdot(\boldsymbol{v}_i + \boldsymbol{v}_j)\boldsymbol{r}_{ij}\Big] \tag{7}$$

where $\boldsymbol{e}_i$ is the total per-atom energy, $\boldsymbol{F}_{ij}$ is the force between atoms i and j, $\boldsymbol{v}_i$ and $\boldsymbol{v}_j$ are their velocities. Finally, $\boldsymbol{r}_{ij}$ is the distance between atoms i and j.

The solution of Eq. 6 is well-known. In our calculations the usage of "centroid/stress/atom" option integrated in LAMMPS simulation package [48, 49] was considered. The obtained data for thermal conductivity, κ, MD and experimental [32, 50] ones, as a function of temperature, T are plotted in Fig. 6. First, let us analyse a reduced temperature range (i.e. [295-310 K]) where comparisons can be made between both approaches. In this range temperature is above liquid-solid phase transition of n-hexadecane. Here, in liquid state, thermal conductivity evaluation by both approaches matches. We can observe that thermal conductivity remains constant around 0.14 W m^{-1}K^{-1} in the studied temperature range.

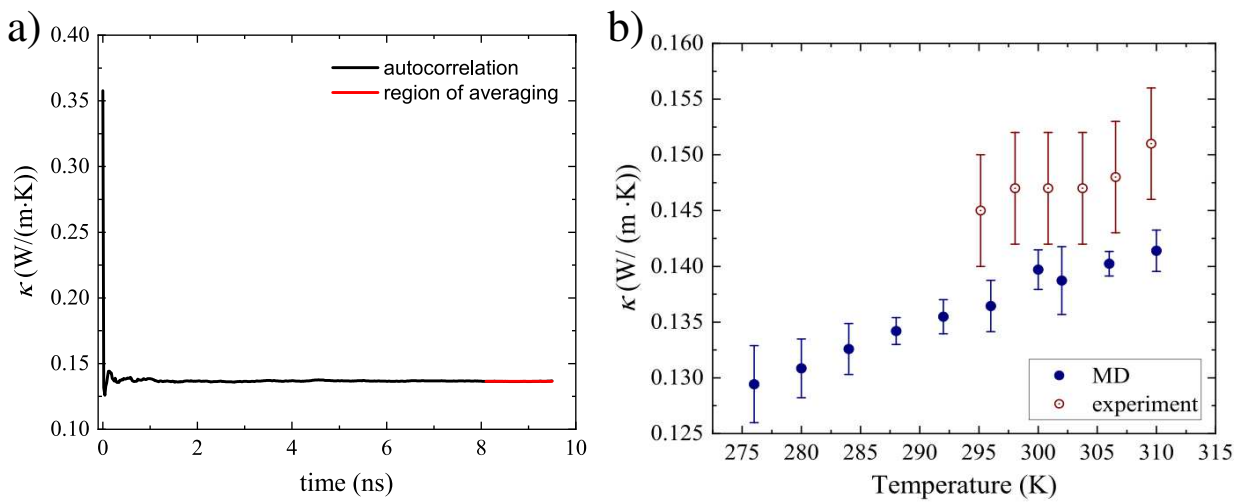

Figure 6: a) Autocorrelation thermal conductivity function obtained for $T = 296$ K. The red line corresponds to the average interval that was used to calculate the mean value shown in Fig. 6 b) and b) Temperature dependence of thermal conductivity, κ, obtained by two different approaches MD (blue dotes) and experiments (maroon dotes).

In the frame of this study, detailed simulation by MD of liquid-solid phase transition features was not done as the crystalline-like structure of the solid phase on n-hexadecane cannot be recovered from the chosen initial liquid state. As a result, the majority of the comparisons were made using our MD simulations and our own experimental data, which corresponds to the liquid phase behavior above T=292K. However, numerical simulations allow us to achieve "excursions" into lower temperature regimes, below the transition limit, and thus to extract some insights about physical properties. We perform such calculations where the considered n-hexadecane sample is not in "crystalline solid-state" but rather in an "amorphous state". Such computations were carried out for the thermal conductivity decreasing T till 276K, a temperature much below the liquid-solid transition point. The findings of our MD simulations of thermal conductivity are presented in Figs. 6. A continuous decrease is observed from 310 K to 276 K, except at 302 K where a small increase can be noted. This temperature is closed to the phase transition one. Yet, it remains much lower than the one observed in other experimental studies (see Fig. 3 in ref. [51] for instance). Considering our MD simulation outputs for thermal conductivity, we can assume that phase transition should occur in the range of $T \in (296, 302)$ K as expected from literature.

4.3 Constant pressure and volume heat capacities

Heat capacities at constant pressure (isobar), C_p, and constant volume (isochor), C_v have been also investigated by means of atomic scale simulations. Molar isochore heat capacity at temperature T, can be related to the system energy fluctuations, in the canonical ensemble it can be calculated as [52]:

$$C_v(T) = \frac{\sigma_E^2}{k_B T^2}, \tag{8}$$

where σ_E^2 is the variance of the total energy, k_B is the Boltzman's constant. The variance of the total energy, σ_E^2, was obtained from the simulation data that were kept after the final NVT production run (see sec. 3.2) with the use of refs. [53, 54] approaches. As it can be seen from the sec. 3.2, after the production run the set of energies, $E(t)$ as a function of time, t, was obtained for each configuration. With the use of trivial relation to obtain variance, we calculated σ_E^2 at each temperature in a row:

$$\sigma_E^2 = \frac{1}{n-1} \sum^{n} \left(E_i - \overline{E}\right)^2$$

where n is the number of points in a set, and overbar corresponds to the mean value.

On the other hand, for "thermostated systems" one can obtain constant volume heat capacity C_v through the long-time averaging of $C_v(t)$ in steady-state regime [52]. The last one can be obtained in terms of energy correlation function, $C_E(t)$ [55] with the use of fluctuation-dissipation theorem [56, 57, 58]:

$$C_v(t) = \frac{1}{k_B T^2} \left(C_E(0) - C_E(t)\right) \tag{9}$$

where $C_E(t)$ is the autocorrelation function of the total energy, defined as:

$$C_E(t) = \langle \delta E(t+t')\delta E(t') \rangle \tag{10}$$

where $\langle ... \rangle$ is the ensemble averaging (averaging over the m-independent configurations), $\delta E(t) = E(t) - \langle E \rangle$ is the total energy fluctuation term, and $< E >$ is the time- and ensemble-averaged value of the total energy. It is also important to underline that Eq. 9 is only relevant for long enough simulation times (higher than the typical relaxation time of the system [52]). Isochore heat capacities obtained by the two approaches (Eq. 8 and Eq. 9) are plotted in Fig. 7 for temperature in the range from $T \in [288, 310]$K. Both theoretical methods provide very similar results with relative discrepancies remain below 10%. Here, there is no noticeable variation of C_v that might inform us about possible phase transition and reorganization of the atomic configuration. Besides, no experimental values are available to assess the reliability of the latter calculations. Thus, we will investigate constant pressure heat capacity C_p for which differential calorimetry experiments were conducted. Finally, taking into account well known equation

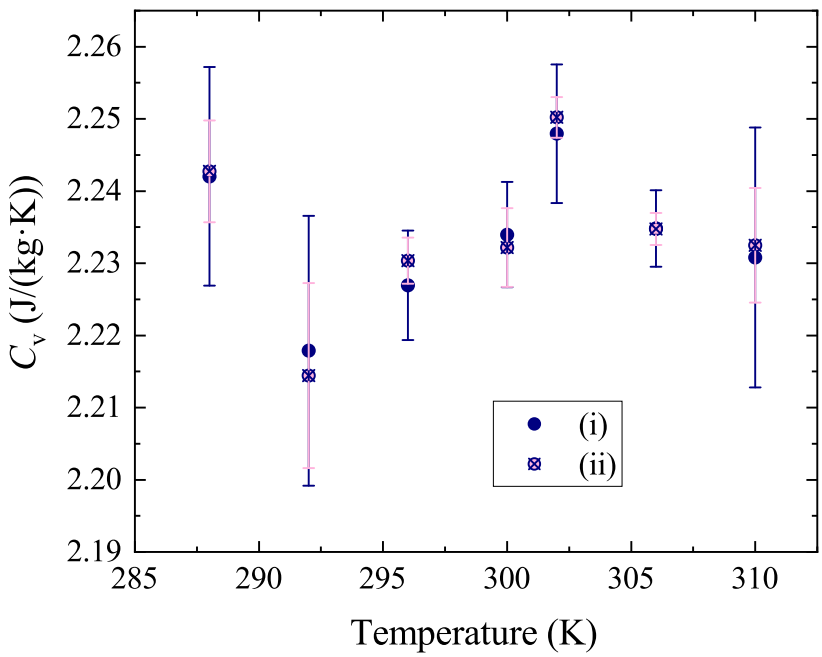

Figure 7: Constant volume molar heat capacity C_v as a function of temperature: i) total energy variation (Eq. 8), and ii) total energy autocorrelation (Eq. 9).

from statistical physics that connects isobare heat capacity and enthalpy, H, one can obtain isobar heat capasity:

$$C_p = \left(\frac{\partial H}{\partial T}\right)_p \tag{11}$$

where $H = E + pV$, where p is the pressure of the system. To have a proper variation of H, we performed additional coolings in isobaric-isothermal ensemble for $t = 2 \times 10^6$ fs. During this runs, each configuration at whole temperature set was cooled up to $T_f = 270$ K with keeping the information about enthalpy and temperature change every $\delta t = 10^4$ fs. Then, a slope of H vs. T corresponds to the foreseen value of C_p.

In Fig. 8 are reported constant pressure heat capacities experimentally and numerically. As previously, experiments were done in the liquid state while simulation data were evaluated from amorphous (280 K) to liquid (310 K) states. In addition to the overall good agreement between DSC and MD, one can clearly see a small pic in C_p at 292 K, in a region where the liquid/amorphous transition occurs. It can be explained as follows: cooling toward samples state transition temperature leads to the breaking of ergodisity of the system. That means that there is not enough time for the system to explore the phase space, and system's configurational degrees of freedom are not accessible anymore [59, 60]. In other words, the experimental time is smaller than the time required for an amorphous system to explore the phase space. The system is confined to the phase space's local energy minima with a decreased number of degrees of freedom compared to those that are available to the system at equilibrium and contribute to the specific heat. This explains why c_p decreases dramatically while cooling approaches state transition temperature T_g(and reaches approximately the same value in the crystal phase).

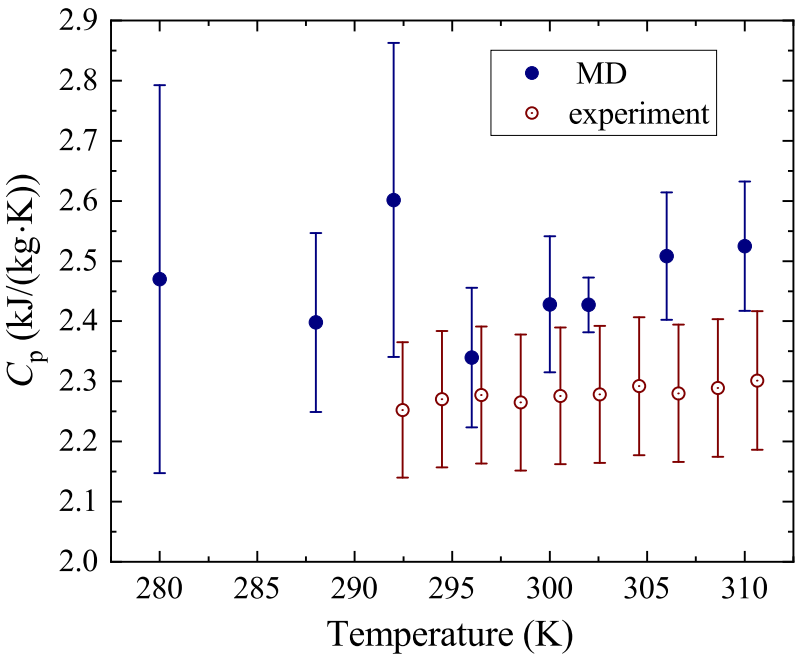

Figure 8: Temperature dependence of isobar molar heat capacity, $C_p(T)$, of n-hexadecane molecules obtained with MD simulations and experiments.

4.4 Mass diffusivity

The study of atom motions give us some useful insights about dynamical properties of the system. Among them, mass diffusivity can be related to the mean-square displacement (MSD) of particles which can be obtained through time average of atom location as:

$$\mathrm{MSD}(t) = \frac{1}{N}\sum_i \left\langle \left(\boldsymbol{r}_i\left(t+t_0\right) - \boldsymbol{r}_i\left(t_0\right)\right)^2 \right\rangle \tag{12}$$

where $\boldsymbol{r}_i\left(t_0\right)$ is the position of ith particle, N is the number of particles, t_0 is an initial time, and brackets $\langle ... \rangle$ correspond to an average over the initial time t_0. For our system the calculation of MSD, over the center of mass of molecules, was performed. Under this assumption, $\boldsymbol{r}_i\left(t_0\right)$, and N in Eq. 12 were replaced by the position of center of mass of ith molecule, and thus N becomes the number of molecules.

When the system reaches steady state (i.e. for times t longer compared to the relaxation time), MSD increases linearly with t in a liquid as the diffusive motion dominates the ballistic one). This can be explained by slowing down of the dynamics with decreasing the temperature T, leading to emergence of an intermediate plateau regime [59]. In this case the slope of MSD is proportional to the diffusion coefficient D:

$$\mathrm{MSD}(t) = 2dDt \tag{13}$$

where $d = 3$ is the space dimension of the considered system. Besides, in the case of MD simulations with periodic boundary conditions, it was found that the final value of diffusion coefficient, D, needs to be corrected by following term [61] which takes into account the size of the box and the shear viscosity. It reads:

$$D = D_{\mathrm{MSD}} + \frac{k_B T \xi}{6\pi\mu L} \tag{14}$$

where D_{MSD} is the diffusion coefficient of center of mass of n-hexadecane molecules that was calculated from the linear regime of MSD (i.e., slope of MSD(t) in log-log scale is 1 for Eq. 13), $\xi \approx 2.837$ is a dimensionless constant [62, 41, 63], μ is the dynamic viscosity, and L is a box size. In our case the simulated system is a cube of length L, that depends on the chosen temperature: $L(T(K))$: $L(310) = 6.315$nm, $L(306) = 6.306$nm, $L(302) = 6.295$nm, $L(300) = 6.291$nm, $L(296) = 6.281$nm, and $L(292) = 6.272$nm. Eq. 14 is known as Yeh and Hummer (YH) relationship [62, 41]. Experimental and numerically assessed value of hexadecane mass diffusivity D as a function of temperature are shown in Fig. 9. It can be noted that both techniques agreed even if MD results exhibit larger uncertainties. In addition, a clear increase of the mass diffusivity is observed while temperature increases as expected.

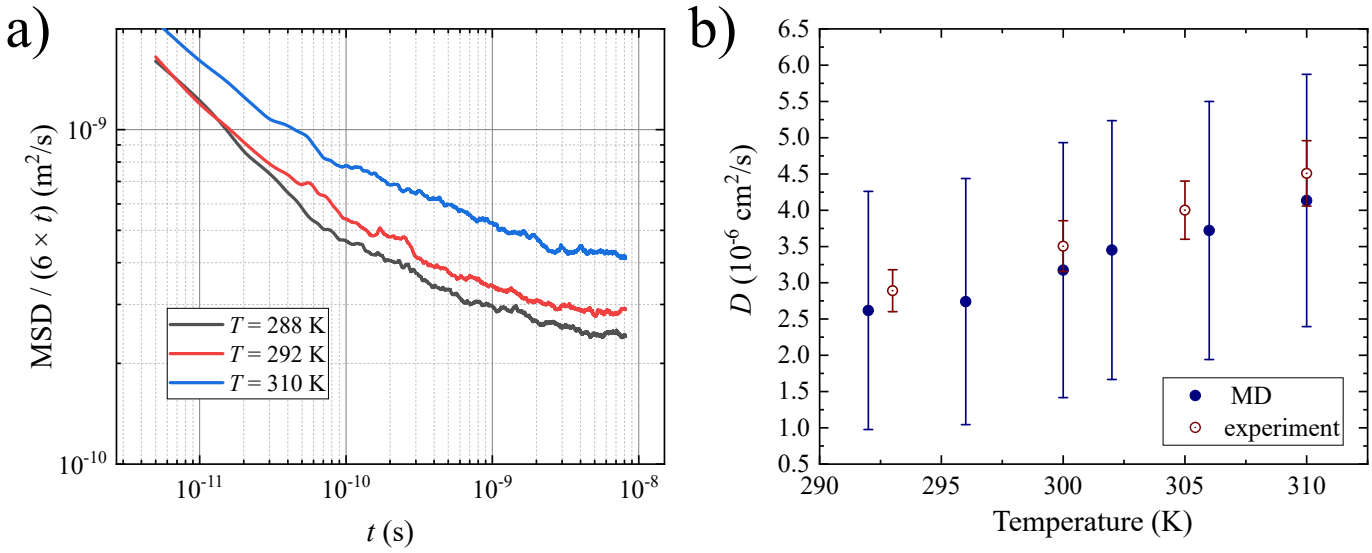

Figure 9: Temperature dependence of: a) MSD and b) diffusion coefficient of center mass of n-hexadecane molecules obtained with MD simulations.

5 Conclusions

This paper is devoted to the investigation of several quantities which describe thermal, mass and momentum transport in PCMs. More precisely, we studied thermophysical and rheological properties for n-hexadecane system at various temperatures using two frameworks - numerical and experimental one. It was shown that the protocol developed for MD simulations allows us to evaluate these physical parameters for different temperature regimes in liquid and amourphous states.

Moreover, we demonstrate that the data for viscosity and other physical quantities such as isobar and isochor heat capacities, coefficient of thermal expansion, diffusion coefficient are all of the same order of magnitude and show good quantitative agreement between each other.

As a conclusion, MD simulations accurately depict the behavior of the liquid phase near the phase transition point of PCMs, and the obtained results can serve as a foundation for further research of the PCMs-based nanocomposite characteristics. Further investigations will have to adress PCM crystallization. This remains a computing challenge which we intend to tackle in future works.

6 Acknwolegement

This paper contains the results obtained in the frames of the project “Hotline” ANR-19-CE09-0003 and DropSurf ANR-20-CE05-0030. This work was performed using HPC resources from GENCI-TGCC and GENCI-IDRIS (2021-A0110913052), in addition HPC resources were partially provided by the EXPLOR centre hosted by the Universitté de Lorraine. Thanks to “STOCK NRJ” that is co-financed by the European Union within the framework of the Program FEDER-FSE Lorraine and Massif des Vosges 2014–2020.

References

[1] J. Hu and K.M. Babu. Testing intelligent textiles. In *Fabric Testing*, pages 275–308. Elsevier, 2008.

[2] C.P. Ho, J. Fan, E. Newton, and R. Au. Improving thermal comfort in apparel. In *Improving Comfort in Clothing*, pages 165–181. Elsevier, 2011.

[3] Rishabh Chaturvedi, Anas Islam, and Kamal Sharma. A review on the applications of PCM in thermal storage of solar energy. *Materials Today: Proceedings*, 43:293–297, 2021.

[4] Maryam Abbasi Kamazani and Cyrus Aghanajafi. Numerical simulation of geothermal-PVT hybrid system with PCM storage tank. *International Journal of Energy Research*, October 2021.

[5] Jing Yao, Pengfei Zhu, Leilei Guo, Lian Duan, Zaoxiao Zhang, Sandra Kurko, and Zhen Wu. A continuous hydrogen absorption/desorption model for metal hydride reactor coupled with PCM as heat management and its application in the fuel cell power system. *International Journal of Hydrogen Energy*, 45(52):28087–28099, October 2020.

[6] Mohammed Reza Hajizadeh, Ammar I. Alsabery, Mikhail A. Sheremet, Rakesh Kumar, Z. Li, and Quang-Vu Bach. Nanoparticle impact on discharging of PCM through a thermal storage involving numerical modeling for heat transfer and irreversibility. *Powder Technology*, 376:424–437, October 2020.

[7] Piao Cheng, Xiao Chen, Hongyi Gao, Xiaowei Zhang, Zhaodi Tang, Ang Li, and Ge Wang. Different dimensional nanoadditives for thermal conductivity enhancement of phase change materials: Fundamentals and applications. *Nano Energy*, 85:105948, July 2021.

[8] Mehdi Esapour, Arash Hamzehnezhad, A. Ali Rabienataj Darzi, and Mahmoud Jourabian. Melting and solidification of PCM embedded in porous metal foam in horizontal multi-tube heat storage system. *Energy Conversion and Management*, 171:398–410, September 2018.

[9] M.E. Nakhchi and J.A. Esfahani. Improving the melting performance of PCM thermal energy storage with novel stepped fins. *Journal of Energy Storage*, 30:101424, August 2020.

[10] A. Safari, R. Saidur, F.A. Sulaiman, Yan Xu, and Joe Dong. A review on supercooling of phase change materials in thermal energy storage systems. *Renewable and Sustainable Energy Reviews*, 70:905–919, April 2017.

[11] N. Beaupere, U. Soupremanien, and L. Zalewski. Nucleation triggering methods in supercooled phase change materials (PCM), a review. *Thermochimica Acta*, 670:184–201, December 2018.

[12] M. Isaiev, X. Wang, K. Termentzidis, and D. Lacroix. Thermal transport enhancement of hybrid nanocomposites; impact of confined water inside nanoporous silicon. *Applied Physics Letters*, 117(3):033701, July 2020.

[13] C.Y. Zhao, Y.B. Tao, and Y.S. Yu. Molecular dynamics simulation of nanoparticle effect on melting enthalpy of paraffin phase change material. *International Journal of Heat and Mass Transfer*, 150:119382, April 2020.

[14] Xiaoxin Yan, Yanhui Feng, Lin Qiu, and Xinxin Zhang. Thermal conductivity and phase change characteristics of hierarchical porous diamond/erythritol composite phase change materials. *Energy*, 233:121158, October 2021.

[15] Dianne J. Luning Prak, Judith A. Harrison, and Brian H. Morrow. Thermophysical properties of two-component mixtures of n-nonylbenzene or 1, 3, 5-triisopropylbenzene with n-hexadecane or n-dodecane at 0.1 MPa: Experimentally measured densities, viscosities, and speeds of sound and molecular packing modeled using molecular dynamics simulations. *Journal of Chemical & Engineering Data*, 66(3):1442–1456, February 2021.

[16] Muxing Zhang, Changling Wang, Ailian Luo, Zhenghao Liu, and Xiaosong Zhang. Molecular dynamics simulation on thermophysics of paraffin/EVA/graphene nanocomposites as phase change materials. *Applied Thermal Engineering*, 166:114639, February 2020.

[17] C. Y. Zhao, Y. B. Tao, and Y. S. Yu. Thermal conductivity enhancement of phase change material with charged nanoparticle: A molecular dynamics simulation. *Energy*, 242:1–8, 2022.

[18] Judith A. Morrow, Brian H.and Harrison. Evaluating the ability of selected force fields to simulate hydrocarbons as a function of temperature and pressure using molecular dynamics. *Energy & Fuels*, 35(5):3742–3752, Mar 2021.

[19] C.Y. Zhao, Y.B. Tao, and Y.S. Yu. Molecular dynamics simulation of thermal and phonon transport characteristics of nanocomposite phase change material. *Journal of Molecular Liquids*, 329:115448, May 2021.

[20] Brian H. Morrow, Sabina Maskey, Micah Z. Gustafson, Dianne J. Luning Prak, and Judith A. Harrison. Impact of molecular structure on properties of n-hexadecane and alkylbenzene binary mixtures. *The Journal of Physical Chemistry B*, 122(25):6595–6603, June 2018.

[21] Luisa F Cabeza, Camila Barreneche, Ingrid Martorell, Laia Miró, Sana Sari-Bey, Magali Fois, Halime O Paksoy, Nurten Sahan, Robert Weber, Mariaella Constantinescu, et al. Unconventional experimental technologies available for phase change materials (pcm) characterization. part 1. thermophysical properties. *Renewable and Sustainable Energy Reviews*, 43:1399–1414, 2015.

[22] Moritz Faden, Stephan Höhlein, Joschka Wanner, Andreas König-Haagen, and Dieter Brüggemann. Review of thermophysical property data of octadecane for phase-change studies. *Materials*, 12(18), 2019.

[23] A Inés Fernández, Aran Solé, Jessica Giró-Paloma, Mònica Martínez, Mila Hadjieva, Abdel Boudenne, Mariaella Constantinescu, Elena Maria Anghel, Marta Malikova, Igor Krupa, et al. Unconventional experimental technologies used for phase change materials (pcm) characterization: part 2–morphological and structural characterization, physico-chemical stability and mechanical properties. *Renewable and Sustainable Energy Reviews*, 43:1415–1426, 2015.

[24] Nicolò R. Sgreva, Justine Noel, Christel Métivier, Philippe Marchal, Hadrien Chaynes, Mykola Isaiev, and Yves Jannot. Thermo-physical characterization of hexadecane during the solid/liquid phase change. *Thermochimica Acta*, February 2022.

[25] J. Noel, Y. Jannot, C. Métivier, and N. Sgreva. Thermal properties of polyethylene glycol 600 in liquid, solid phases and through the phase transitionn, under revisions for thermochimica acta.

[26] Ryoji Mitsuhashi, Yuta Suzuki, Yusuke Yamanari, Hiroki Mitamura, Takashi Kambe, Naoshi Ikeda, Hideki Okamoto, Akihiko Fujiwara, Minoru Yamaji, Naoko Kawasaki, Yutaka Maniwa, and Yoshihiro Kubozono. Superconductivity in alkali-metal-doped picene. *Nature*, 464(7285):76–79, Mar 2010.

[27] Anish Tuteja, Wonjae Choi, Minglin Ma, Joseph M. Mabry, Sarah A. Mazzella, Gregory C. Rutledge, Gareth H. McKinley, and Robert E. Cohen. Designing superoleophobic surfaces. *Science*, 318(5856):1618–1622, 2007.

[28] Ibtissem Chriaa, Abdelwaheb Trigui, Mustapha Karkri, Ilyes Jedidi, Makki Abdelmouleh, and Chokri Boudaya. Thermal properties of shape-stabilized phase change materials based on low density polyethylene, hexadecane and SEBS for thermal energy storage. *Applied Thermal Engineering*, 171:115072, May 2020.

[29] Frances D. Lenahan, Michael Zikeli, Michael H. Rausch, Tobias Klein, and Andreas P. Fröba. Viscosity, Interfacial Tension, and Density of Binary-Liquid Mixtures of n-Hexadecane with n-Octacosane, 2,2,4,4,6,8,8-Heptamethylnonane, or 1-Hexadecanol at Temperatures between 298.15 and 573.15 K by Surface Light Scattering and Equilibrium Molecular Dynamics Simulations. *Journal of Chemical and Engineering Data*, 66(5):2264–2280, 2021.

[30] Guilherme C.Q. da Silva, Fernanda G. Oliveira, Wladmir F. de Souza, Marcia C.K. de Oliveira, Pierre M. Esteves, and Bruno A.C. Horta. Effects of paraffin, fatty acid and long alkyl chain phenol on the solidification of n-hexadecane under harsh subcooling condition: A molecular dynamics simulation study. *Fuel*, 285(September 2020):119029, 2021.

[31] P Espeau, L Robles, D Mondieig, Y Haget, MA Cuevas-Diarte, and HAJ Oonk. Mise au point sur le comportement énergétique et cristallographique des n-alcanes-i. série de c8h18 à c21h44. *Journal de chimie physique*, 93:1217–1238, 1996.

[32] C. Vélez, M. Khayet, and J.M. Ortiz de Zárate. Temperature-dependent thermal properties of solid/liquid phase change even-numbered n-alkanes: n-hexadecane, n-octadecane and n-eicosane. *Applied Energy*, 143:383–394, 2015.

[33] Yves Jannot and Alain Degiovanni. *Thermal properties measurement of materials*. ISTE ; WILEY, January 2018. Pages: 342 pages.

[34] J. E. Tanner. Use of the stimulated echo in NMR diffusion studies. *The Journal of Chemical Physics*, 52(5):2523–2526, March 1970.

[35] E. O. Stejskal and J. E. Tanner. Spin Diffusion Measurements: Spin Echoes in the Presence of a Time-Dependent Field Gradient. *The Journal of Chemical Physics*, 42(1):288–292, January 1965.

[36] L. Martínez, R. Andrade, E. G. Birgin, and J. M. Martínez. Packmol: A package for building initial configurations for molecular dynamics simulations. *Journal of Computational Chemistry*, 30(13):2157–2164, 2009.

[37] William Humphrey, Andrew Dalke, and Klaus Schulten. VMD – Visual Molecular Dynamics. *Journal of Molecular Graphics*, 14:33–38, 1996.

[38] John Stone. *An Efficient Library for Parallel Ray Tracing and Animation.* Master's thesis, Computer Science Department, University of Missouri-Rolla, April 1998.

[39] Large-scale atomic/molecular massively parallel simulator. `https://www.lammps.org`.

[40] Shirley W. I. Siu, Kristyna Pluhackova, and Rainer A. Böckmann. Optimization of the opls-aa force field for long hydrocarbons. *Journal of Chemical Theory and Computation*, 8(4):1459–1470, 2012. PMID: 26596756.

[41] Othonas A. Moultos, Yong Zhang, Ioannis N. Tsimpanogiannis, Ioannis G. Economou, and Edward J. Maginn. System-size corrections for self-diffusion coefficients calculated from molecular dynamics simulations: The case of CO2, n-alkanes, and poly(ethylene glycol) dimethyl ethers. *The Journal of Chemical Physics*, 145(7):074109, August 2016.

[42] Konstantinos D. Papavasileiou, Loukas D. Peristeras, Andreas Bick, and Ioannis G. Economou. Molecular dynamics simulation of pure n-alkanes and their mixtures at elevated temperatures using atomistic and coarse-grained force fields. *The Journal of Physical Chemistry B*, 123(29):6229–6243, Jul 2019.

[43] Alessio David, Antonio De Nicola, Ugo Tartaglino, Giuseppe Milano, and Guido Raos. Viscoelasticity of short polymer liquids from atomistic simulations. *Journal of The Electrochemical Society*, 166:B3246–B3256, 01 2019.

[44] Shirley W. I. Siu, Kristyna Pluhackova, and Rainer A. Böckmann. Optimization of the opls-aa force field for long hydrocarbons. *Journal of Chemical Theory and Computation*, 8(4):1459–1470, Apr 2012.

[45] Jean-Paul Ryckaert, Giovanni Ciccotti, and Herman J.C Berendsen. Numerical integration of the cartesian equations of motion of a system with constraints: molecular dynamics of n-alkanes. *Journal of Computational Physics*, 23(3):327–341, 1977.

[46] Shuichi Nosé. A unified formulation of the constant temperature molecular dynamics methods. *The Journal of Chemical Physics*, 81(1):511–519, 1984.

[47] Krishan Lal, Neelima Tripathi, and Gyan P. Dubey. Densities, viscosities, and refractive indices of binary liquid mixtures of hexane, decane, hexadecane, and squalane with benzene at 298.15 k. *Journal of Chemical & Engineering Data*, 45(5):961–964, August 2000.

[48] Paul Boone, Hasan Babaei, and Christopher E. Wilmer. Heat flux for many-body interactions: Corrections to lammps. *Journal of Chemical Theory and Computation*, 15(10):5579–5587, 2019. PMID: 31369260.

[49] Donatas Surblys, Hiroki Matsubara, Gota Kikugawa, and Taku Ohara. Application of atomic stress to compute heat flux via molecular dynamics for systems with many-body interactions. *Phys. Rev. E*, 99:051301, May 2019.

[50] J. Noel, C. Métivier, S. Becker, and S. Leclerc. Natural convection in phase change material: Experimental study. *International Journal of Heat and Mass Transfer*, 183:122047, 2022.

[51] Diego Vasco, Manuel Muñoz, Paula Galvez, and Paula A Zapata. Modification of cu and cuo nanoparticles with oleic acid and thermal characterization of paraffins: towards the preparation of a stable nanopcm. 11 2015.

[52] L. Klochko, J. Baschnagel, J. P. Wittmer, and A. N. Semenov. General relations to obtain the time-dependent heat capacity from isothermal simulations. *The Journal of Chemical Physics*, 154(16):164501, 2021.

[53] G. George, L. Klochko, A. N. Semenov, J. Baschnagel, and J. P. Wittmer. Ensemble fluctuations matter for variances of macroscopic variables. *The European Physical Journal E*, 44(2):13, Mar 2021.

[54] G. George, L. Klochko, A. N. Semenov, J. Baschnagel, and J. P. Wittmer. Fluctuations of non-ergodic stochastic processes. *The European Physical Journal E*, 44(4):54, Apr 2021.

[55] Johannes K. Nielsen and Jeppe C. Dyre. Fluctuation-dissipation theorem for frequency-dependent specific heat. *Physical Review B*, 54(22):15754–15761, December 1996.

[56] Theory of simple liquids. In Jean-Pierre Hansen and Ian R. McDonald, editors, *Theory of Simple Liquids (Fourth Edition)*, page i. Academic Press, Oxford, fourth edition edition, 2013.

[57] Copyright. In L.D. LANDAU and E.M. LIFSHITZ, editors, *Statistical Physics (Third Edition)*, page iv. Butterworth-Heinemann, Oxford, third edition edition, 1980.

[58] C. Ruscher, A. N. Semenov, J. Baschnagel, and J. Farago. Anomalous sound attenuation in voronoi liquid. *The Journal of Chemical Physics*, 146(14):144502, April 2017.

[59] Andrea Cavagna. Supercooled liquids for pedestrians. *Physics Reports*, 476(4):51–124, 2009.

[60] Walter. Kauzmann. The nature of the glassy state and the behavior of liquids at low temperatures. *Chemical Reviews*, 43(2):219–256, Oct 1948.

[61] Alessandro Perego and Fardin Khabaz. Thermodynamics, dynamics, and rheology of fuel surrogates: Application of the time–temperature superposition principle in molecular dynamics simulations. *Energy & Fuels*, 34(9):10631–10640, Sep 2020.

[62] In-Chul Yeh and Gerhard Hummer. System-size dependence of diffusion coefficients and viscosities from molecular dynamics simulations with periodic boundary conditions. *The Journal of Physical Chemistry B*, 108(40):15873–15879, Oct 2004.

[63] Gabriela Guevara-Carrion, Jadran Vrabec, and Hans Hasse. Prediction of self-diffusion coefficient and shear viscosity of water and its binary mixtures with methanol and ethanol by molecular simulation. *The Journal of Chemical Physics*, 134(7):074508, February 2011.